Journal of Alloys and Compounds 505 (2010) 393–399

Contents lists available at ScienceDirect

Journal of Alloys and Compounds

journal homepage: www.elsevier.com/locate/jallcom

Electrical resistivity and Mössbauer effect investigations on $Tb_{0.27}Dy_{0.73}(Mn_{1-x}Fe_x)_2$ intermetallics

W. Bodnar[a], P. Stoch[b,c], J. Chmist[a], J. Pszczoła[a,*], P. Zachariasz[b], J. Suwalski[b]

[a] Faculty of Physics and Applied Computer Science, AGH, Al. Mickiewicza 30, 30-059 Kraków, Poland
[b] Institute of Atomic Energy, 05-400 Świerk-Otwock, Poland
[c] Faculty of Materials Science and Ceramics, AGH, Al. Mickiewicza 30, 30-059 Kraków, Poland

ARTICLE INFO

Article history:
Received 27 April 2010
Received in revised form 23 May 2010
Accepted 29 May 2010
Available online 19 June 2010

PACS:
75.50.Gg
61.66.Dk
72.15.Eb
75.30.Kz
76.80.+y

Keywords:
Intermetallics
Terfenol-D
Crystal structure
Electrical resistivity
Curie temperatures
Mössbauer effect
Magnetic hyperfine field

ABSTRACT

This paper concerns synthesis, X-ray analysis (300 K), electrical resistivity and ^{57}Fe Mössbauer effect studies (4.2 K) of complete $Tb_{0.27}Dy_{0.73}(Mn_{1-x}Fe_x)_2$ intermetallic series, with a borderline compound $Tb_{0.27}Dy_{0.73}Fe_2$ known as Terfenol-D. A cubic Laves phase *Fd*3*m* of the $MgCu_2$-type is observed across the series. The lattice parameter decreases parabolically with *x*. Electrical resistivity was measured in a wide temperature region across the $Tb_{0.27}Dy_{0.73}(Mn_{1-x}Fe_x)_2$ series and the parameters which characterize resistivity dependence on temperature, including Debye temperature, were determined. Residual, phonon and magnetic contributions were separated from electrical resistivity. The magnetic contribution to electrical resistivity was applied to estimate Curie temperatures. The Curie temperature increases significantly with *x*. ^{57}Fe Mössbauer effect measurements for the $Tb_{0.27}Dy_{0.73}(Mn_{1-x}Fe_x)_2$ intermetallic system evidence an [1 0 0] easy axis of magnetization. Mn/Fe substitution introduces a local area, at sub-nanoscale, with different Mn/Fe neighbourhoods of the tested ^{57}Fe atoms. Hyperfine interaction parameters, an isomer shift, a magnetic hyperfine field and a quadrupole interaction parameter were determined from the spectra both for the local neighbourhood area and, as averaged values, for the sample as bulk. The average magnetic hyperfine field increases parabolically with *x*. The correlation between Curie temperatures and magnetic hyperfine fields is discussed.

© 2010 Elsevier B.V. All rights reserved.

1. Introduction

The heavy rare earth (R)–transition metal (M) magnetic intermetallics of Laves phases, RM_2-type, are widely studied for both their fundamental interest and for their practical applications [1–5].

The ferrimagnetism of R–M compounds is a result of rare earth 4f(5d) electron magnetism and transition metal 3d electron magnetism [6,7].

For practical reasons, RFe_2 type materials have previously been studied because of their strong magnetostriction [8]. It has been found that in intermetallics of the $Tb_{1-x}Dy_xFe_2$ type with Tb/Dy substitution in the R-sublattice, strong magnetostriction with minimum magnetocrystaline anisotropy has been approached for the $Tb_{0.27}Dy_{0.73}Fe_2$ compound, often commercially called Terfenol-D [8].

Recently both Terfenol-D and other intermetallics of the series $Tb_xDy_{1-x}Fe_2$ have been intensively tested as strongly magnetostrictive candidates for composites with piezoceramics or polymers in order to obtain materials with a giant magnetoelectric effect [9–11].

The presence of Mn and Fe atoms in the M-sublattice has previously been experimentally studied in the $Dy(Mn_{1-x}Fe_x)_2$ and $Dy(Mn_{0.4-x}Al_xFe_{0.6})_2$ intermetallic series by electric resistivity measurements and the ^{57}Fe Mössbauer effect [12,13].

Substitution of one transition metal for another in the RM_2 system can be treated as a driving force to change the number *n* of 3d electrons (calculated per transition metal atom) and thus, to change band properties and the magnetic, electric and hyperfine interaction properties which are related to them [7].

In fact, the electrical properties of R–M intermetallics are less known and the source of these properties and their relations to R–M magnetism would seem still to be open to research. Therefore, it was interesting to study the influence of the 3d-band electron population on the electrical properties and magnetism of the M-sublattice and especially on the hyperfine interaction parameters

* Corresponding author.
E-mail address: pszczola@agh.edu.pl (J. Pszczoła).

0925-8388/$ – see front matter © 2010 Elsevier B.V. All rights reserved.
doi:10.1016/j.jallcom.2010.05.178

in the Mn/Fe substituted series $Tb_{0.27}Dy_{0.73}(Mn_{1-x}Fe_x)_2$ of intermetallics which ends with the $Tb_{0.27}Dy_{0.73}Fe_2$ compound, one of the best of the new magnetostrictive materials. For this purpose the series $Tb_{0.27}Dy_{0.73}(Mn_{1-x}Fe_x)_2$ was prepared and X-ray analysis, electrical resistivity and ^{57}Fe Mössbauer effect measurements were performed.

2. Materials and crystal structure

Polycrystalline intermetallics $Tb_{0.27}Dy_{0.73}(Mn_{1-x}Fe_x)_2$ (x = 0, 0.2, 0.4, 0.6, 0.8 and 1) were synthesized by arc melting with contact-less ignition in an inert, high purity argon atmosphere using appropriate amounts of the metals Tb, Dy (99.9% purity), Mn and Fe (99.99% purity) [14]. For the sake of homogenization, the obtained ingots were annealed in vacuum at 1123 K for 2 h and then cooled down along with the furnace (cooling: approximately 250 K/h).

Next, the compounds were powdered and their phase homogeneity and crystal structure were tested with standard X-ray diffraction measurements using Mo K_α radiation. The X-ray diffractograms were analyzed numerically using a Rietveld-type fitting procedure, adopting both the $K_{\alpha1}$ (wavelength λ_1 = 0.70930 Å) and $K_{\alpha2}$ (wavelength λ_2 = 0.71359 Å) lines [15].

A cubic, *Fd*3*m*, $MgCu_2$-type C15 clean crystal phase was observed for all compounds. It will be helpful to recall that in the C15 crystal structure each transition metal atom is surrounded by six other transition metal atoms as nearest neighbours [1,16]. The C15-Laves phase structure has been described in detail elsewhere [1,16].

Since the atomic radius of Mn (r_{Mn} = 1.79 Å) is larger than the corresponding radius of Fe (r_{Fe} = 1.72 Å) [17], the unit cell parameter a, described by the fitted expression $a(x) = (-0.049x^3 + 0.173x^2 - 0.401x + 7.613)$ Å (Fig. 1, curve 1), reduces softly non-linearly with composition parameter x (bottom axis) or the average number n of 3d electrons (top axis). The maximal error value equals Δa = 0.002 Å. Fig. 1 also shows some fragmentary literature data on the unit cell parameter for $Tb_{0.27}Dy_{0.73}(Mn_{1-x}Fe_x)_2$ compounds [18,19].

The upper horizontal axis in Fig. 1 shows the number n of 3d electrons calculated per transition metal atom following the formula $n(x) = 5(1-x) + 6x$, in line with the stoichiometry of the $Tb_{0.27}Dy_{0.73}(Mn_{1-x}Fe_x)_2$ series, where 5 and 6 are the numbers of 3d electrons for Mn and Fe atoms, respectively.

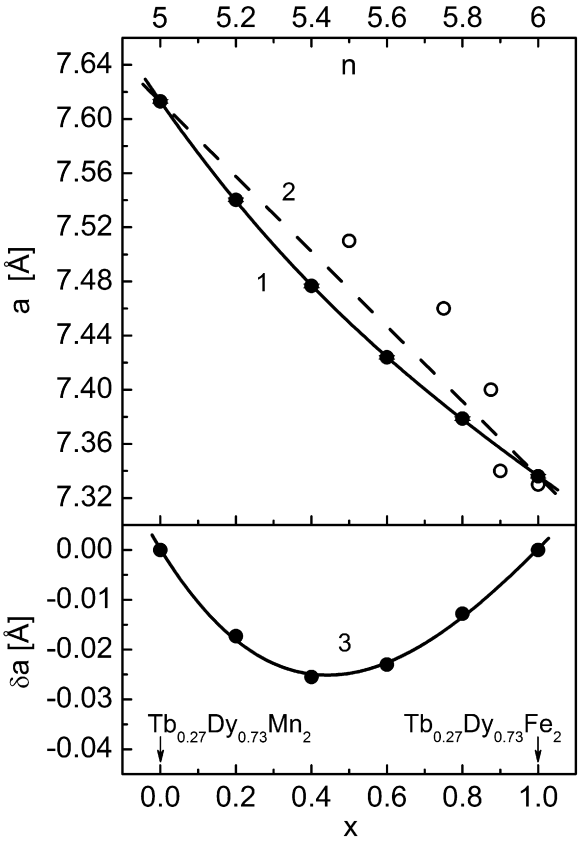

Fig. 1. Unit cell parameters a (curve 1), calculated Vegard parameters a_V (dashed line 2) and their difference δa (curve 3) for the $Tb_{0.27}Dy_{0.73}(Mn_{1-x}Fe_x)_2$ intermetallic system (300 K) against composition parameter x (bottom axis) and the average number n of 3d electrons (top axis). Open marks denote data from literature [18,19].

A concave deviation for $a(x)$ from the Vegard rule i.e. from linear dependence (Fig. 1, dashed line 2) occurs. The a_V values of the unit cell parameter corresponding to the Vegard rule can be calculated following the formula $a_V(x) = (-0.277x + 7.613)$ Å (Fig. 1, dashed line 2). It is interesting to present the difference $\delta a = a - a_V$ between the experimentally obtained unit cell parameters a and the unit cell parameters a_V which correspond to them, as presented in Fig. 1, curve 3. Curve 3 is described by the following numerical formula $\delta a(x) = (-0.0480x^3 + 0.1721x^2 - 0.1241x + 0.0003)$ Å. A minimum value of the fitted curve 3 appears for $x \simeq 0.45$. This concave deviation, which is negative in its values, between the experimental a and the Vegard rule following a_V is probably caused by a magnetovolume effect [19].

3. Electrical resistivity studies

3.1. Resistivities

For electrical resistivity measurements, bar (cuboid) shaped specimens with typical dimensions of 1 mm × 1 mm × 15 mm were delicately and precisely cut from the ingots using a precise diamond wheel saw.

During sample preparation it has been found that the $Tb_{0.27}Dy_{0.73}Mn_2$ compound is fragile whereas the $Tb_{0.27}Dy_{0.73}Fe_2$ compound is not brittle. The fragility is reduced as a result of Mn/Fe substitution across the $Tb_{0.27}Dy_{0.73}(Mn_{1-x}Fe_x)_2$ series.

Electrical contacts to the bars were attached by point spark-welding of high purity thin copper wires onto the ends of the bars. Only microscopically observed crack free samples were used for the measurements. A four point AC method was used at temperatures below ambient temperature and a DC method with commutated current above this temperature. The experimental data of both methods were found to match each other at the same temperature in the common temperature region. The good quality dependencies of electrical resistivity ρ vs. temperature T for the $Tb_{0.27}Dy_{0.73}(Mn_{1-x}Fe_x)_2$ series are shown in Fig. 2.

The resistivity observed for magnetic materials can be expressed by the Matthiesen formula [12,20,21]

$$\rho = \rho_0 + \rho_f + \rho_m \tag{1}$$

where ρ_0 is the residual resistivity, ρ_f is the phonon scattering resistivity described by the Bloch–Grüneisen formula [12,20,21] and ρ_m is the magnetic contribution to total resistivity. The particular resistivity contributions present in the Matthiesen formula have been discussed previously [12,20,21]. A numerical approach to separate ρ_0, ρ_f, ρ_m and to determine the parameters characterising these components has been described in detail elsewhere [12].

As discussed previously, in the case of R–M intermetallics expression (1) for temperatures $T \ll \theta_D$ and $T \ll T_C$ (θ_D is the Debye temperature, T_C is the Curie temperature) can be rewritten in the following form [12,20]

$$\rho(T) = 497.6D\left(\frac{T}{\theta_D}\right)^5 + AT^2 + BT + \rho_0 \tag{2}$$

where A, B and D are parameters.

In a high temperature range ($T \gg T_C$) the total resistivity formula can be approximated as [12,20,21]

$$\rho(T) = D\left(\frac{T}{\theta_D}\right) + C \tag{3}$$

where C is a parameter.

An analogous method of calculations following formulae (1)–(3), as described elsewhere [12], was applied to separate particular contributions to total electrical resistivity. The results of resistivity measurements and of numerical calculations are presented in Figs. 3 and 4 and in Table 1.

The residual resistivity ρ_0 as a function of composition parameter x for the $Tb_{0.27}Dy_{0.73}(Mn_{1-x}Fe_x)_2$ series is presented in Fig. 3, curve 1. Residual resistivity ρ_0 decreases parabolically with x and can be approximated by the numerical formula

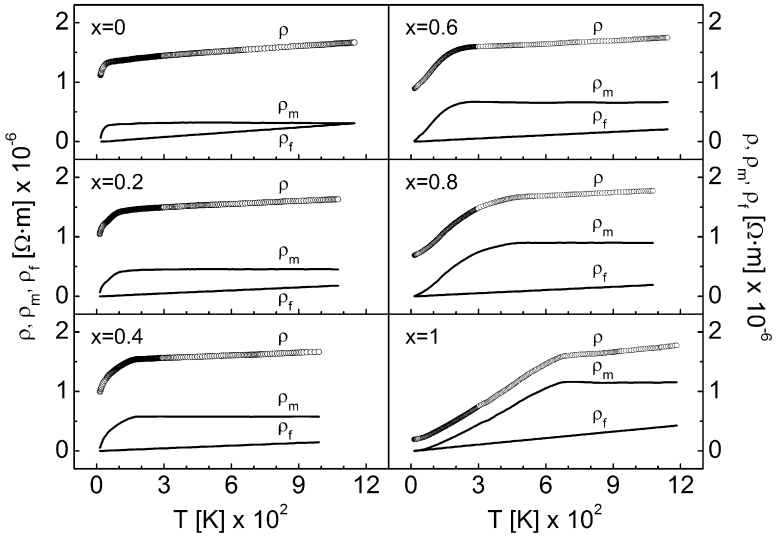

Fig. 2. Electrical resistivities: the total ρ, the phonon ρ_f and the magnetic ρ_m observed against temperature for the $Tb_{0.27}Dy_{0.73}(Mn_{1-x}Fe_x)_2$ intermetallic system.

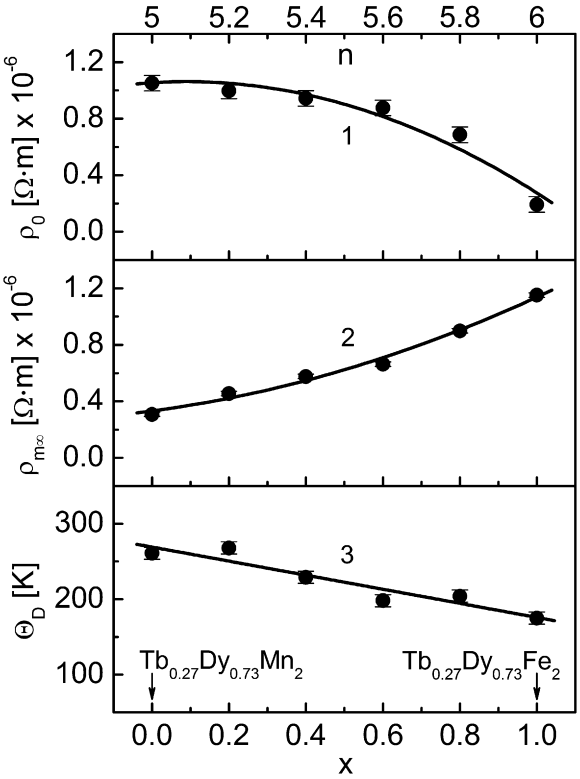

Fig. 3. Residual resistivity ρ_0 (curve 1), asymptotic magnetic resistivity $\rho_{m\infty}$ (curve 2) and the Debye temperature θ_D (line 3) for the $Tb_{0.27}Dy_{0.73}(Mn_{1-x}Fe_x)_2$ series against composition parameter x (bottom axis) and the average number n of 3d electrons (top axis).

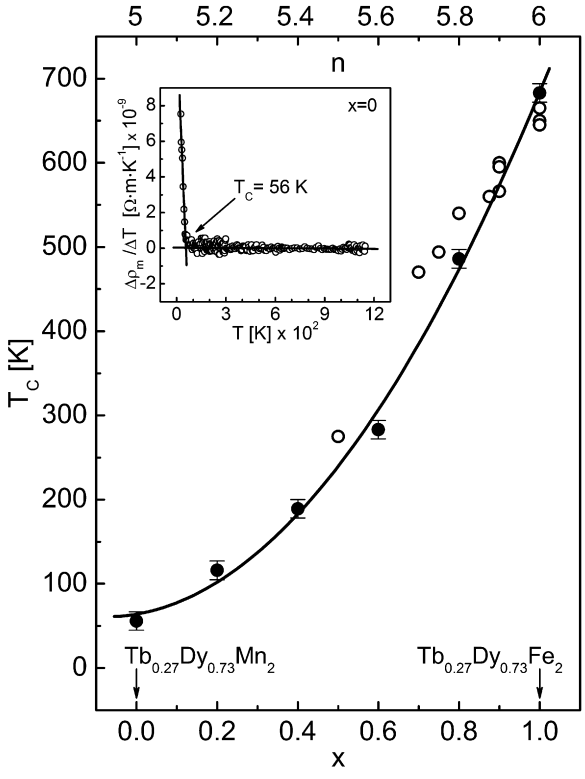

Fig. 4. The Curie temperatures T_C of the $Tb_{0.27}Dy_{0.73}(Mn_{1-x}Fe_x)_2$ series against composition parameter x (bottom axis) and the average number n of 3d electrons (top axis). Open marks denote literature data [18,19,27,28]. Insert: an exemplary $\Delta\rho_m / \Delta T$ function of temperature for the $Tb_{0.27}Dy_{0.73}Mn_2$ compound. Line–line intersection determines the Curie temperature T_C.

Table 1
Electrical resistivity parameters for $Tb_{0.27}Dy_{0.73}(Mn_{1-x}Fe_x)_2$ intermetallics.

x	n	A $[\Omega\,m/K^2] \times 10^{-10}$	B $[\Omega\,m/K] \times 10^{-9}$	C $[\Omega\,m] \times 10^{-6}$	D $[\Omega\,m] \times 10^{-10}$
0	5	2.625	−0.631	1.364	701.040
0.2	5.2	1.626	0.213	1.452	447.650
0.4	5.4	3.714	1.893	1.518	338.935
0.6	5.6	0.934	−0.282	1.537	360.503
0.8	5.8	0.513	−0.294	1.585	361.991
1	6	0.052	0.211	1.341	630.075

$\rho_0(x) = (-0.95x^2 + 0.17x + 1.05)\,\Omega\,m \times 10^{-6}$ (Fig. 3, curve 1). The maximal error value equals $\Delta\rho_0 = 0.06\,\Omega\,m \times 10^{-6}$. As a rule, residual resistivity originates from both crystal lattice imperfections and statistical imperfections caused by a random distribution of atoms [22]. In this case, the statistical imperfections should be related to the presence of randomly distributed Tb and Dy atoms in the R-sublattice and randomly distributed Mn and Fe atoms in the M-sublattice. Tb/Dy disorder, if any, can be assumed to be practically the same across the series. Moreover, in Tb and Dy the same $5d^16^2$ external electrons screen the core atomic shell and they mainly correspond to electron–electron scattering. Therefore, contributions to ρ_0 from Tb and Dy should be comparable. Thus it can be expected that ρ_0 arises predominantly from crystal imperfections rather than statistical disorder. As $Tb_{0.27}Dy_{0.73}Mn_2$ is more fragile than $Tb_{0.27}Dy_{0.73}Fe_2$, it can be deduced that the crystal imperfections in the former predominate over their counterparts in the latter. As a result, the ρ_0 for $Tb_{0.27}Dy_{0.73}Mn_2$ is higher than the ρ_0 value for $Tb_{0.27}Dy_{0.73}Fe_2$. In these circumstances the expected Mn/Fe statistical disorder introduces only a convex deviation from the linearity observed for $\rho_0(x)$, which may be interpreted tentatively as the counterpart of a maximum.

The high temperature asymptotic values $\rho_{m\infty} = \rho_m(T \to +\infty)$ of magnetic resistivity for the $Tb_{0.27}Dy_{0.73}(Mn_{1-x}Fe_x)_2$ series are presented in Fig. 3, curve 2. The $\rho_{m\infty}$ resistivity grows softly parabolically with composition parameter x and can be approximated by the numerical formula $\rho_{m\infty}(x) = (0.44x^2 + 0.36x + 0.33)\,\Omega\,m \times 10^{-6}$. The maximal error value equals $\Delta\rho_{m\infty} = 0.02\,\Omega\,m \times 10^{-6}$. This tendency can be understood given that the number of transition metal magnetic scattering centers (magnetic moments) increases with x. Indeed, the Mn atom's magnetic moment in C15-type RMn_2 intermetallics strongly depends on $d_{Mn-Mn} = a\sqrt{2}/4$, the nearest neighbour interatomic Mn–Mn distance [18,19,23–26]. There is a certain critical distance, $d_c = 2.66$ Å, above which Mn atoms carry a large and stable magnetic moment. This occurs in the $TbMn_2$ compound [23–25]. For compounds with $d_{Mn-Mn} < d_c$ a mixture is established, with either small, or no, magnetic moments at all at the Mn sites very much as in the case of the $DyMn_2$ compound, which is almost at the border line with d_{Mn-Mn}, just below d_c [24–26]. Assuming that the pseudobinary compound $Tb_{0.27}Dy_{0.73}Mn_2$ is a stoichiometrical mixture of the $TbMn_2$ and $DyMn_2$ compounds, it can be expected that some of the Mn atoms carry a stable magnetic moment. The introduction of Fe atom magnetic moments into the M-sublattice stabilizes all atom magnetic moments. Thus the number of scattering centers (stable magnetic moments) rises with Mn/Fe replacement in the $Tb_{0.27}Dy_{0.73}(Mn_{1-x}Fe_x)_2$ series and the growing tendency in $\rho_{m\infty}(x)$ is consequently observed.

The Debye temperatures θ_D of the $Tb_{0.27}Dy_{0.73}(Mn_{1-x}Fe_x)_2$ compounds are shown in Fig. 3, line 3. The points are approximated by the numerical formula $\theta_D(x) = (-93x + 269)$ K. The maximal error value equals $\Delta\theta_D = 8$ K. A tendency to slightly decrease with x may be observed. These θ_D values are situated below the Debye temperatures known for Mn (400–450 K) and Fe (420–467 K), and above the values known for Tb (158 K) and Dy (140–158 K) metals [20].

3.2. Curie temperatures

The dependence $\rho_m(T)$ can be used to find the magnetic ordering temperatures of the studied intermetallic series following a method previously presented elsewhere [12,21]. The magnetic ordering temperature T_C is situated in a temperature range with a maximal change in numerically estimated parameter $\Delta\rho_m / \Delta T$ as presented in the inset of Fig. 4 for the $Tb_{0.27}Dy_{0.73}Mn_2$ compound. The intersection of the two fitted straight lines determines the magnetic ordering temperature. Experimental error depends on the quality of $\Delta\rho_m / \Delta T$ dependence and maximal error can be expressed as $\Delta T_C = 11$ K. The Curie temperature T_C dependence against composition parameter x and the average number n of 3d electrons for the $Tb_{0.27}Dy_{0.73}(Mn_{1-x}Fe_x)_2$ series is presented in Fig. 4. The relatively low Curie temperature for $x = 0$ (56 K) shows a strong increase across the series up to $x = 1$ (683 K). Experimental points follow well the numerical formula $T_C(x) = (538x^2 + 82x + 64)$ K. Fig. 4 also contains fragmentary literature data [18,19,27,28].

4. ^{57}Fe Mössbauer effect studies

4.1. Spectra analysis

The ^{57}Fe Mössbauer effect transmission spectra of the $Tb_{0.27}Dy_{0.73}(Mn_{1-x}Fe_x)_2$ series, presented in Fig. 5, were collected at 4.2 K by using a standard transmission technique with a ^{57}Co in the Pd source [29]. Spectra characteristic of an [1 0 0] easy axis of magnetization were fitted assuming a random distribution of the Mn and Fe atoms in the transition metal sublattice.

As in the $MgCu_2$-type crystal lattice, the transition metal atom is surrounded by six transition metal atoms as nearest neighbours [1,16], so that the random distribution of the Mn/Fe atoms causes different neighbourhoods of the probed Fe atom, which can be surrounded by $(6-k)$ Mn atoms and k Fe atoms ($k = 0, 1, 2, \ldots, 6$). A particular Mn/Fe nearest neighbour coordination produces locally its own Mössbauer effect subspectrum contributing to the measured Mössbauer effect pattern, and therefore determines its

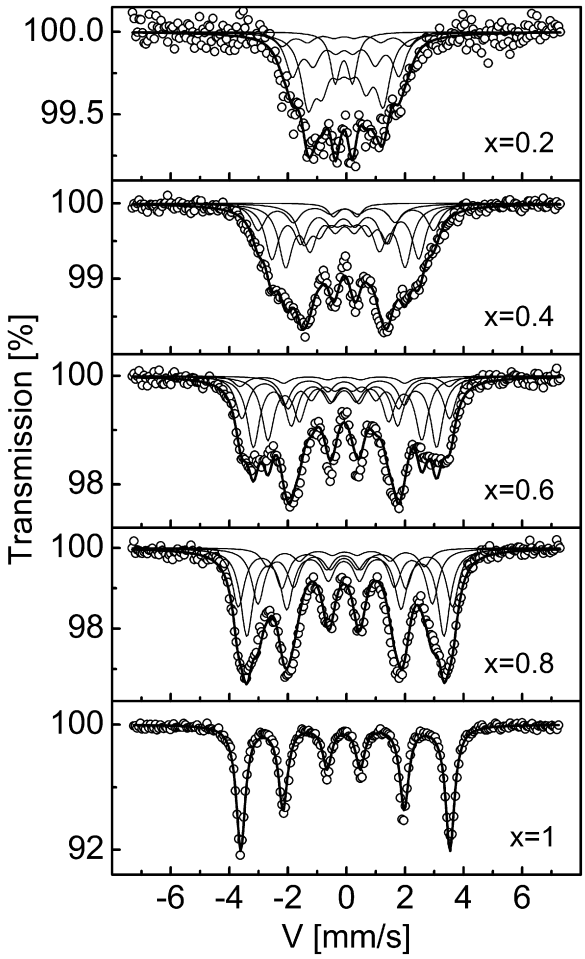

Fig. 5. ^{57}Fe Mössbauer effect transmission spectra of the $Tb_{0.27}Dy_{0.73}(Mn_{1-x}Fe_x)_2$ intermetallic series (4.2 K).

own hyperfine interaction parameters. The probability of particular Mn/Fe nearest neighbourhoods and their Mössbauer subspectra is expressed by a Bernoulli distribution formula [30]:

$$P(6;k) = \frac{6!}{(6-k)!k!}(1-x)^{6-k}x^k \quad (4)$$

which in this form is adapted for the intermetallic series $Tb_{0.27}Dy_{0.73}(Mn_{1-x}Fe_x)_2$. Considering the above M-sublattice randomness it was assumed that the amplitudes of particular Mössbauer subspectra follow probabilities $P(6;k)$. In order to reduce the number of fitted parameters, surroundings with probabilities of less than 0.1 of maximal probability $P(6;k)$ were neglected and for this reason, the remaining probabilities were normalized again.

Exemplary values of the parameters describing the quality of the fitting procedure for the compound $Tb_{0.27}Dy_{0.73}(Mn_{0.6}Fe_{0.4})_2$ are equal to $\chi^2 = 1.533$ and $MISFIT = 0.213$. The parameters for the other compounds of the series are similar to these exemplary data. It is worth adding that the hyperfine field average numerical error obtained from the fitting procedure equals $\Delta(\mu_0 H_{hf}) = 0.18T$ (μ_0 is the vacuum permeability).

It can be seen that for the compounds $Tb_{0.27}Dy_{0.73}(Mn_{0.8}Fe_{0.2})_2$ and $Tb_{0.27}Dy_{0.73}(Mn_{0.6}Fe_{0.4})_2$ with six Mn atoms as nearest neighbours there is no magnetic hyperfine interaction at the tested Fe nuclei and consequently only a quadrupole doublet is observed.

4.2. Local magnetic hyperfine fields

The locally originated magnetic hyperfine fields $\mu_0 H_{hf}$ corresponding to particular Mössbauer subspectra of the $Tb_{0.27}Dy_{0.73}(Mn_{1-x}Fe_x)_2$ series, resulting from the fitting procedure, labeled by x and treated as functions of number k, are presented in Fig. 6 (upper case). It is worth noticing that the value $k/6$ can be interpreted as a local composition parameter in the first coordination.

Additionally, the upper case of Fig. 6 (dotted curve 1) shows magnetic hyperfine fields $\mu_0 H_{hf}$ arithmetically averaged over x against the number k. It can be seen that the magnetic hyperfine field $\mu_0 H_{hf}$ (arithmetically averaged over x) (Fig. 6, dotted curve 1) increases parabolically with k and is described by the numerical formula $\mu_0 H_{hf}(k) = (-0.29k^2 + 4.91k + 3.55)T$.

It is interesting to present the particular, or locally originated, magnetic hyperfine field data again in the lower case of Fig. 6. In this case the local $\mu_0 H_{hf}$ fields, ascribed to corresponding k values, are presented across the series. The dotted curve 2 in Fig. 6 shows the weighted average value of the magnetic hyperfine field, calculated for each x, using the corresponding Bernoulli distribution as in formula (4).

4.3. Average hyperfine interaction parameters

Fig. 7 shows the average hyperfine interaction parameters weighted by subspectra amplitudes, calculated in line with the Bernoulli distribution function, i.e. the isomer shift IS (with respect

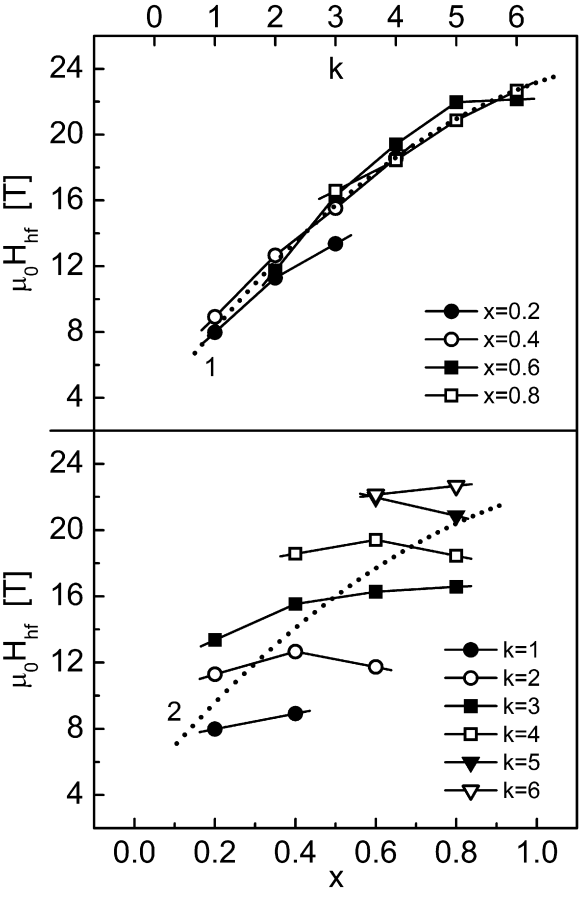

Fig. 6. Local magnetic hyperfine fields $\mu_0 H_{hf}$ for the $Tb_{0.27}Dy_{0.73}(Mn_{1-x}Fe_x)_2$ series: labelled by x as functions of k (upper case), values averaged arithmetically over x (dotted curve 1), labelled by k as functions of x (lower case), weighted average values (dotted curve 2).

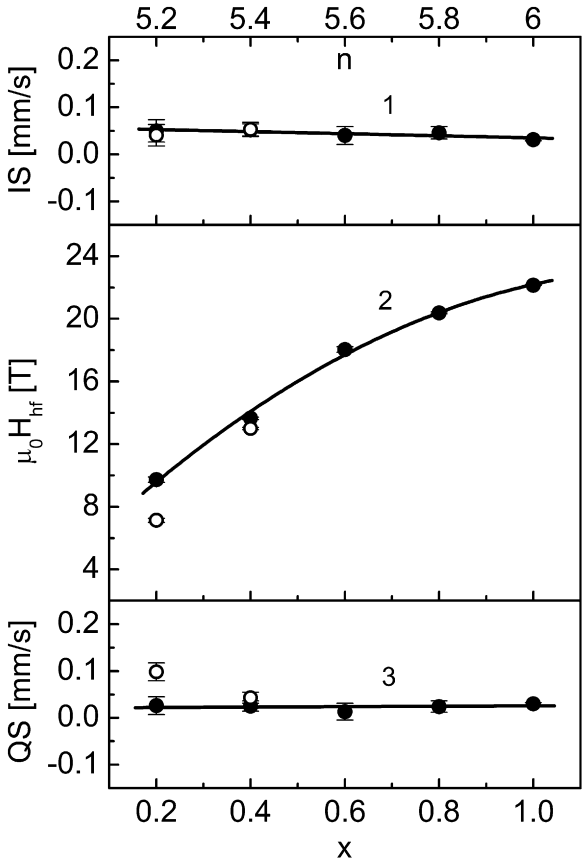

Fig. 7. Hyperfine interaction parameters of the $Tb_{0.27}Dy_{0.73}(Mn_{1-x}Fe_x)_2$ series at 4.2 K: the isomer shift *IS* (line 1), the magnetic hyperfine field $\mu_0 H_{hf}$ (curve 2) and the quadrupole interaction parameter *QS* (line 3) vs. composition parameter x (bottom axis) and the average number n of 3d electrons (top axis). Open marks denote average values for the sample as bulk.

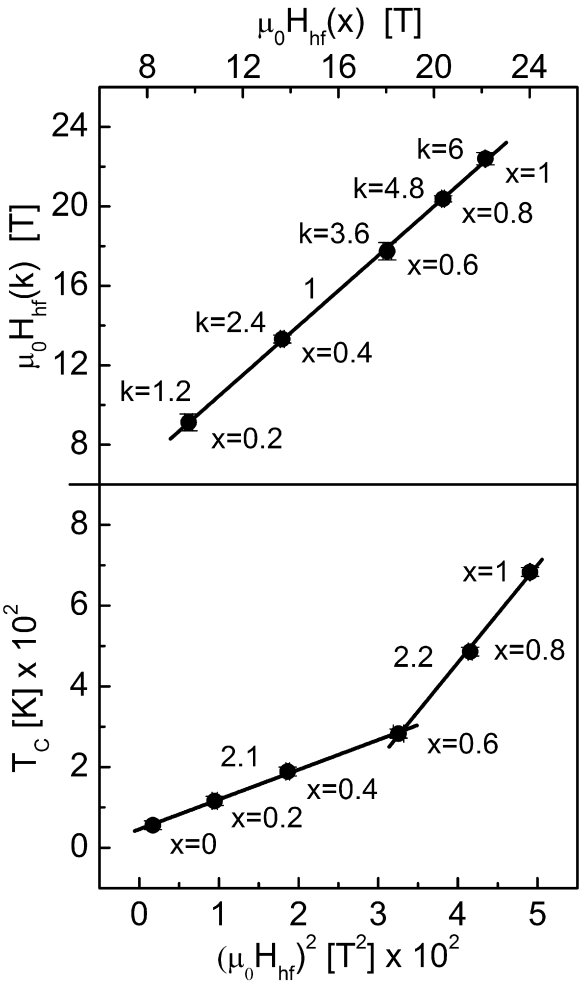

Fig. 8. Upper case: correlation between the arithmetically averaged magnetic hyperfine field $\mu_0 H_{hf}(k)$ and the weighted magnetic hyperfine field $\mu_0 H_{hf}(x)$ for the $Tb_{0.27}Dy_{0.73}(Mn_{1-x}Fe_x)_2$ series. The points are labelled by corresponding k and x values. Lower case: correlation between the Curie temperature T_C and the square value $(\mu_0 H_{hf})^2$ of the magnetic hyperfine field for the $Tb_{0.27}Dy_{0.73}(Mn_{1-x}Fe_x)_2$ series. The points are labelled by corresponding x values.

to iron metal, at 300 K), the magnetic hyperfine field $\mu_0 H_{hf}$, and the quadrupole interaction parameter QS [31], determined for the $Tb_{0.27}Dy_{0.73}(Mn_{1-x}Fe_x)_2$ intermetallics at 4.2 K as a function of composition parameter x (bottom axis) or the average number n of 3d electrons (top axis). The black points in Fig. 7 presented for $x = 0.2$ and $x = 0.4$ are average values corresponding only to the magnetic surroundings, whereas the open points correspond to average values calculated including also the non-magnetic case characteristic of surroundings with only Mn atoms in the nearest neighbourhood of the probed Fe atom. It is interesting to notice that the magnetic hyperfine field $\mu_0 H_{hf}$ numerically extrapolated to $x = 0$, which equals 4.14T, corresponds satisfactorily to the average field 6.93T observed for the doped $Dy(^{57}Fe\underline{Mn})_2$ system and to the field 6.63 T which occurs for the $Tb(^{57}Fe\underline{Mn})_2$ system [25,26].

The isomer shift IS is almost constant with composition parameter x and follows the numerical formula $IS(x) = (-0.022x + 0.057)$ mm / s (Fig. 7, line 1).

The weighted average $\mu_0 H_{hf}$ increases parabolically with composition parameter x and is described by the numerical formula $\mu_0 H_{hf}(x) = (-11.34x^2 + 29.39x + 4.14)T$ (Fig. 7, curve 2). Since for most $Tb_{0.27}Dy_{0.73}(Mn_{1-x}Fe_x)_2$ compounds Curie temperatures are relatively high (Fig. 4), the measured magnetic hyperfine fields should correspond to magnetic moments at 4.2 K, which are not far from their magnetic saturation values. This is not necessarily the case for the Mn-rich compounds; for low x-values (low Curie temperatures, Fig. 4) the magnetic moments and the magnetic hyperfine fields which correspond to them at 4.2 K can be somewhat distant from their saturation values.

The quadrupole parameter QS changes only slightly with x and can be described by the numerical expression $QS(x) = (0.005x + 0.021)$ mm / s (Fig. 7, line 3).

4.4. Correlation between the magnetic fields

It is interesting to make a comparison of the average local magnetic hyperfine field $\mu_0 H_{hf}$ as a function of k (taken from Fig. 6, dotted curve 1) and the weighted average magnetic hyperfine field $\mu_0 H_{hf}$ as a function of x (Fig. 7, curve 2) as presented in the upper case of Fig. 8. Points are described by the corresponding k and x numbers. The k-values used in Fig. 8 (upper case) are calculated applying the proportion $x : 1 = k : 6$ where, as mentioned previously, 6 denotes the number of crystal lattice nearest neighbours surrounding the studied Fe atom, and k is the average number of Fe atoms (not necessarily in this case an integral number) in neighbour coordination [1,2,16]. It can be seen that a linear correlation between $\mu_0 H_{hf}(k)$ and $\mu_0 H_{hf}(x)$ appears. The resulting $\mu_0 H_{hf}(k)$ vs. $\mu_0 H_{hf}(x)$ dependence obeys the numerical expression: $\mu_0 H_{hf}(k) = (1.06\mu_0 H_{hf}(x) - 1.21)T$ (Fig. 8, line 1).

5. Summary and discussion

In this work, a complete series of intermetallics $Tb_{0.27}Dy_{0.73}(Mn_{1-x}Fe_x)_2$ was prepared for the first time, and X-ray analysis at 300 K was performed. Crystal structure and unit cell parameter a were determined.

Electrical resistivity measurements were performed and the parameters describing electrical resistivity were obtained. A separated magnetic resistivity contribution was applied to determine the Curie temperatures T_C of the complete $Tb_{0.27}Dy_{0.73}(Mn_{1-x}Fe_x)_2$ series.

From ^{57}Fe Mössbauer effect studies at 4.2 K, hyperfine interaction parameters observed locally for different nearest neighbour configurations of the tested ^{57}Fe atom, and the average hyperfine interaction parameters for the sample as bulk have been determined. A direct linear correlation between the arithmetically averaged magnetic hyperfine field $\mu_0 H_{hf}(k)$ and the weighted magnetic hyperfine field $\mu_0 H_{hf}(x)$ is observed.

As is presented in Fig. 4, the magnetic ordering temperature T_C strongly varies across the $Tb_{0.27}Dy_{0.73}(Mn_{1-x}Fe_x)_2$ series. Since a rigorous expression for the magnetic ordering temperature related to the band structure of metallic ferromagnets or ferrimagnets has not been formulated up to date, it is not an easy task to explain the tremendous change in the Curie temperature which is observed. Considering an approximate additive formula for the Curie temperature of intermetallics $T_C = T_R + T_M$ (T_R is the rare earth sublattice contribution approximately constant across the series, T_M is the transition metal sublattice contribution) [1,3,32] it can be expected that Mn/Fe substitution modifies the density of 3d states, especially 3d states at Fermi level; that it modifies the integral of exchange interactions, the splitting energy between the 3d subbands, the transition metal magnetic moment, and thus it effects mainly the T_M contribution to the Curie temperature across the series.

Assuming roughly that the Curie temperature contribution T_M can be seen as $k_B T_M \sim J_{M-M}\, m_M\, m_M$ [33], where J_{M-M} is the average exchange integral between M–M neighbours, m_M is the average magnetic moment per transition metal atom and k_B is the Boltzmann constant, a correlation between T_C and $\mu_0 H_{hf}$ can be considered.

It has previously been observed that in substituted RM_2-type intermetallics the magnetic hyperfine field $\mu_0 H_{hf}$ is proportional to the average magnetic moment m_M calculated per transition metal atom [29]. Thus in the lower case of Fig. 8 the correlation between T_C and $(\mu_0 H_{hf})^2$ is presented. Points are labeled by corresponding x numbers. It should be added that the value of $\mu_0 H_{hf}$ for $x = 0$ is the result of numerical extrapolation using curve 2 from Fig. 7.

The Curie temperature T_C increases with the $(\mu_0 H_{hf})^2$ parameter, and two linear sections can be adjusted to this dependence with an inflexion point present for $x = 0.6$. Those sections are described by the following numerical formulae: $T_C = [0.74(\mu_0 H_{hf})^2 + 45.98]$ K (Fig. 8, line segment 2.1) and $T_C = [2.42(\mu_0 H_{hf})^2 - 508.16]$ K (Fig. 8, line segment 2.2). It can be noticed that the slope rate of line segment 2.2 is approximately three times higher then the slope rate of line segment 2.1. It should be marked here that magnetic moments m_M and magnetic hyperfine fields $\mu_0 H_{hf}$ (which correspond to them) for the Fe poor area of the $Tb_{0.27}Dy_{0.73}(Mn_{1-x}Fe_x)_2$ series are not close to the point of magnetic saturation. T_C growth can be caused by the growth of the m_M magnetic moment. At this stage the magnetic moment of iron m_{Fe} oversteps the magnetic moment of manganese m_{Mn} and the Fe contribution in the M-sublattice increases with x. Moreover the average J_{M-M} exchange integral grows across the series, since it can be expected that J_{Fe-Fe} is many times higher than J_{Mn-Mn}. Indeed the Curie temperature $k_B T_C(RFe_2) \sim J_{Fe-Fe}\, m_{Fe}\, m_{Fe}$ is higher than $k_B T_C(RMn_2) \sim J_{Mn-Mn}\, m_{Mn}\, m_{Mn}$ (Fig. 4) [1,2].

It should be added that a more exhaustive discussion of Curie temperatures could be possible with the knowledge of the band structure and exchange interactions for compounds of the series in question.

Acknowledgements

Supported partially by The Polish Ministry of Science and Higher Education, project no. *R*015000504 and partially by *AGH*, project nos. 10.10.220.476 and 11.11.220.01.

References

[1] K.N.R. Taylor, Adv. Phys. 20 (1971) 551.
[2] K.H.J. Buschow, in: E.P. Wohlfarth (Ed.), Ferromagnetic Materials, vol. 1, North-Holland, Amsterdam, 1980.
[3] E. Burzo, H.R. Kirchmayr, in: K.A. Gschneidner Jr., L. Eyring (Eds.), Handbook on the Physics and Chemistry of Rare Earths, vol. 12, North-Holland, Amsterdam, 1989.
[4] E. Burzo, A. Chełkowski, H.R. Kirchmayr, in: O., Madelung, H.P.J., Wijn (Eds.), Landolt-Börnstein Numerical Data and Functional Relationships in Science and Technology, New Series, Group III, vol. 19, subvol. d2, Springer, Berlin, 1990.
[5] A.M. Tishin, Y.I. Spichkin, The Magnetocaloric Effect and its Applications, Institute of Physics Publishing, Bristol, 2003.
[6] I.A. Campbell, J. Phys. F: Met. Phys. 2 (1972) L47.
[7] B. Gicala, J. Pszczoła, Z. Kucharski, J. Suwalski, Phys. Lett. A 185 (1994) 491.
[8] A.E. Clark, E.R. Wohlfarth, Ferromagnetic Materials, vol. 1, North-Holland, Amsterdam, 1980, p. 531.
[9] M. Fiebig, J. Phys. D: Appl. Phys. 38 (2005) R123.
[10] C.W. Nan, G. Liu, Y. Lin, Appl. Phys. Lett. 83 (2003) 4366.
[11] N. Zhang, J. Fan, X. Rong, H. Cao, J. Wei, J. Appl. Phys. 101 (2007) 063907.
[12] P. Stoch, J. Pszczoła, P. Guzdek, J. Chmist, W. Bodnar, A. Jabłońska, J. Suwalski, A. Pańta, J. Alloys Compd. 392 (2005) 62.
[13] P. Stoch, J. Pszczoła, P. Guzdek, M. Wzorek, A. Jabłońska, J. Suwalski, L. Dąbrowski, A. Pańta, J. Alloys Compd. 384 (2004) 25.
[14] P. Stoch, M. Onak, A. Pańta, J. Pszczoła, J. Suwalski, Synthesis and crystal structure of $Dy(Fe–Co–Al)_2$, IEA Monographs, vol. 5, Institute of Atomic Energy, Otwock-Świerk, 2002.
[15] J. Rodriguez-Carvajal, Physica B 192 (1993) 55.
[16] F. Laves, Naturwissenschaften 27 (1939) 65.
[17] Table of Periodic Properties of the Elements, Sargent-Welch Scientific Company, 7300 Linder Ave., Skokie, Ilinois 60077 (1980).
[18] C.H. Wu, X.M. Jin, W.Q. Ge, Y.C. Chuang, X.P. Zhong, R.Q. Li, J.Y. Li, J. Magn. Magn. Mater. 163 (1996) 360.
[19] J. Arout Chelvane, G. Markandeyulu, J. Magn. Magn. Mater. 294 (2005) 298.
[20] F.J. Blatt, Physics of Electronic Conduction in Solids, McGraw-Hill, Michigan, 1968.
[21] W. Vonsovskij, Magnetizm, 1st ed., Nauka, Moscow, 1971 (in Russian).
[22] P. Stoch, J. Pszczoła, P. Guzdek, J. Chmist, A. Pańta, J. Alloys Compd. 394 (2005) 116.
[23] P.J. Brown, B. Ouladdiaf, R. Ballou, J. Deportes, A.S. Markosyan, J. Phys.: Condens. Matter 4 (1992) 1103.
[24] H. Wada, H. Nakamura, K. Yoshimura, M. Shiga, Y. Nakamura, J. Magn. Magn. Mater. 70 (1987) 134.
[25] J. Przewoźnik, J. Żukrowski, K. Krop, Nucl. Instr. Meth. Phys. Res. B 76 (1993) 130.
[26] K. Krop, J. Żukrowski, J. Przewoźnik, J. Marzec, G. Wiesinger, Th. Häufler, G. Hilscher, W. Steiner, J. Magn. Magn. Mater. 147 (1995) 141.
[27] A.E. Clark, J.P. Teter, M. Wun-Fogle, J. Appl. Phys. 69 (1991) 5771.
[28] T. Funayama, T. Kobayashi, I. Sakai, M. Sahashi, Appl. Phys. Lett. 61 (1992) 114.
[29] W. Bodnar, M. Szklarska-Łukasik, P. Stoch, P. Zachariasz, J. Pszczoła, J. Suwalski, J. Alloys Compd. 496 (2010) 37.
[30] W. Feller, An Introduction to Probability Theory and its Applications, vol. 1, 2nd ed., Wiley, London, 1961, p. 175.
[31] G.K. Wertheim, Mössbauer effect, 1st ed., Academic Press, London, 1964.
[32] J. Pszczoła, K. Krop, J. Magn. Magn. Mater. 59 (1986) 95.
[33] A.H. Morrish, The Physical Principles of Magnetism, John Wiley and Sons, Inc., New York, 1965.